ADVANCED HEALTHCARE MATERIALS
www.advhealthmat.c

Prolonged Local In Vivo Delivery of Stimuli-Responsive Nanogels That Rapidly Release Doxorubicin in Triple-Negative Breast Cancer Cells

*Yi Zhang, Pere Dosta, João Conde, Nuria Oliva, Mian Wang, and Natalie Artzi**

Triple negative breast cancer patients remain with chemotherapy as their only viable therapeutic option. However, the toxicity of available anticancer drugs and their inefficient delivery have limited the development of effective chemotherapy administration protocols and combination therapies. Drug delivery devices that can properly target chemotherapy to the right cells with efficient cancer-cell killing may play a vital role in eliminating triple-negative breast cancer. While systemic delivery results in low drug accumulation at the tumor site and for a short period of time, local delivery enables sustained drug release. However, a system that is able to provide rapid, yet prolonged action, would enable efficient tumor elimination. Herein, the development of dual-sensitive nanogels is described that are designed to rapidly dislodge the chemotherapy drug, doxorubicin, inside cancer cells through dual-sensitive action—pH and redox sensitivities—enabling efficient cancer-cell killing while eliminating systemic side effects. Their embedding within a hydrogel injected next to a tumor in a triple-negative breast-cancer mouse model enables prolonged release of the drug with instantaneous action when inside the cells resulting in efficacious tumor elimination compared to sustained local delivery only. This technology can be used for the delivery of combination therapies and for the treatment of other solid tumors.

1. Introduction

Triple-negative breast cancer represents an aggressive malignancy that is not susceptible to hormone inhibition and must therefore be treated with standard first-line chemotherapy, such as doxorubicin. Unfortunately, more than 50% of the patients develop resistance to this intervention, which leaves them with no other option rather than palliative therapy.[1,2] The prolongation of the delivery of an adequate dosage of chemotherapy in tumors, beyond a few hours (as in systemic delivery), can effectively eradicate the cancer cells prior to the development of resistance.[3] Hence, drug delivery devices that can prolong the delivery of a drug and allow for rapid cancer-cell killing may play a vital role in eliminating triple-negative breast cancer.

The use of drug delivery devices, in particular biodegradable polymeric materials, has generated a vast scientific and economic impact on disease therapeutics, especially cancer treatment. Designing an ideal device for the delivery of cancer therapy is complex as there are many aspects to consider. Anticancer therapeutics needs to be well protected by a carrier and highly targeted to the tumor site, and be composed of biocompatible and bioabsorbable materials that can provide with controlled release of therapeutics. To date, the majority of devices for cancer therapy are either in a particulate form (nanoparticles that are mostly administered intravenously),[4,5] or hydrogels that can be implanted to provide local release.[6,7] Both of them have intriguing properties, but inevitable bottlenecks as well. Nanoparticles allow for the protection of encapsulated/conjugated therapeutics with enhanced uptake to cancer cells and provide with flexible design parameters that enable versatility in the type and dosage of cargos to be delivered.[4,8] Much research has been conducted to optimize nanoparticles for efficient cancer therapy. Surface modifications, such as PEGylation, are able to increase the circulation time of nanoparticles.[9] Conjugation with targeting moieties confers higher selectivity than bare nanoparticles that provide passive uptake by the enhanced permeability and retention (EPR) at the tumor site.[10,11] However, the percentage of nanoparticles that eventually reach the

Dr. Y. Zhang, Dr. P. Dosta, Dr. J. Conde, Dr. N. Oliva, Dr. M. Wang, Prof. N. Artzi
Institute for Medical Engineering and Science
Massachusetts Institute of Technology
Cambridge, MA 02139, USA

Dr. P. Dosta, Dr. M. Wang, Prof. N. Artzi
Department of Medicine
Division of Engineering in Medicine
Brigham and Women's Hospital
Harvard Medical School
Boston, MA 02115, USA
E-mail: nartzi@bwh.harvard.edu

Dr. J. Conde
School of Engineering and Materials Science
Queen Mary University of London
London E14NS, UK

Prof. N. Artzi
State Key Laboratory of Molecular Engineering of Polymers
Fudan University
Shanghai 200438, China

The ORCID identification number(s) for the author(s) of this article can be found under https://doi.org/10.1002/adhm.201901101.

DOI: 10.1002/adhm.201901101

tumor is still low. Systemic administration not only mandates higher dose of therapeutics, but also increases the systemic toxicity caused by particles that accumulate in the liver, spleen or kidneys.[11,12] Hydrogels, on the other hand, can serve as reservoirs for a wide range of therapeutics that can be either physically entrapped or chemically conjugated.[2,4] Due to the uniqueness of its fabrication, hydrogels can be implanted or crosslink in situ, at the tumor site.[6,13] Therefore, local delivery of therapeutics may overcome many of the shortcomings of systemic delivery. However, the loading efficiency and homogeneity of hydrophobic drugs may be limited, and as the release of therapeutics highly relies on passive diffusion, a controlled and sustained drug release is hard to achieve, particularly in the case of small molecule therapeutics, like most chemotherapy drugs.[14]

Composite hydrogel materials embedded with drug-loaded micro- or nanoparticles enable overcoming the inherent limitations of systemic nanoparticles delivery or local hydrogel-based delivery of free drugs.[8,15] Composite hydrogels provide two layers of control over drug release kinetics; they help maintain the nanoparticles at the tumor site while tapering their release kinetics, and the nanoparticles further regulate conjugated/encapsulated drug release. Ideally, the release of therapeutics from the cargo should be sustained to provide long-term efficacy, however, once entering the cancer cells, drug release to the cytoplasm should be instantaneous to confer rapid cancer-cell killing. Biosensitive nanoparticles provide a promising way for triggered cancer therapy due to the inherent differences between the healthy and tumoral tissue microenvironments. Materials that are sensitive to those differences can be used to precisely and rapidly deliver therapeutics to cancer cells. Many promising biosensitivity properties have been exploited for cancer treatment.[16] pH sensitive materials have been studied for cancer treatment as the reduced pH at the endosome can help release the drug rapidly.[17–20] In addition, redox sensitivity was exploited as cancer cells contain notably higher intracellular reductant concentration (a sevenfold increase in the case of lung adenocarcinoma cell line) compared to normal cells.[21] Composite hydrogels containing biosensitive nanoparticles can provide a drug delivery depot with triggered release inside cancer cells. To date, there was no report on the formation of cancer-triggered hydrogel composite with embedded nanoparticles that confer dual sensitivity, for example, pH and redox.

Herein, we developed a framework by which to provide efficient cancer therapy that involves two distinct release kinetics profiles. Hydrogel-assisted local delivery of dual-sensitive (redox- and pH) nanogels provides with sustained and localized drug delivery, that upon their uptake into cancer cells undergo rapid disassembly (triggered by the dual stimuli) to trigger the release of the anticancer drug (**Figure 1**).

2. Results and Discussion

Hydrogels presented in this study are composed of oxidized dextran (Dex) forming aldehyde groups, and hydroxylated generation five (G5) dendrimer (Den) with 25% amines on their surface. The crosslinking of Dex:Den hydrogel is derived from the aldehyde-amine Schiff-base reaction to form pH-sensitive imine bonds (Figure 1B).[22,23] Hydrogel degradation kinetics occurs via the cleavage of the imine bond under hydrolytic conditions, and is enhanced in acidic pHs.[24] The hydrogel has been shown to be biocompatible, nonimmunogenic, and was used to successfully deliver drugs and nucleic acids (antisense DNA, miRNAs, and siRNAs) for cancer therapy.[2,23,25–28] In terms of material degradation, previous studies demonstrated that the formulation used is stable for a few weeks, and then the hydrogel degrades back to the original polymers that are excreted from the body.[29]

The dual-sensitive nanogels (DSNGs) developed herein are based on Dex crosslinked with cystamine—a disulfide bond-containing molecule conferring redox sensitivity (Figure 1C). Doxorubicin (Dox), a chemotherapeutic drug, was conjugated to Dex via aldehyde-amine interaction, providing with reversible, pH-sensitive, imine bond.[30] The disulfide bond is cleaved in the presence of the highly concentrated reductant present in cancer cells, such as glutathione (GSH) and dithiothreitol (DTT).[31] Therefore, disulfide bond along with imine bond confer the redox-pH dual sensitivity to the nanogels. Cystamine was replaced by hexasmethylenediamine to fabricate nonredox sensitive nanogels, serving as a control (NSNGs). The aldehyde residues on the surface of the Dex-based nanogels provide with facile interaction with amine containing moieties, such as mono amino-PEG, dye, and a cell- targeting peptide, all of which were used in this study. In the present work, a triple-negative breast cancer cell line, MDA-MB-231 (MDA), was chosen as a tumor model as chemotherapy is the only available therapy for this group of patients.

We confirmed that Dex oxidation and Dex:Dox formation took place by ^{1}H-NMR (300 MHz, DMSO-d_6) (Figure S2, Supporting Information). The dual sensitive nanogels were then fabricated by single-emulsion technique and nanogel size was tuned by water/oil ratio, or polymer/crosslinker ratio. Smaller nanogels were obtained at 1/5 compared to 1/1 water/oil ratio, at a size of 150 and 1000 nm, respectively. However, nonsignificant differences were observed at different polymer crosslinker ratios (Figure S1, Supporting Information). In addition, the morphology of the nanogels was characterized by transmission electron microscopy (TEM). Based on their biophysiochemical properties (Table S1, Supporting Information) 1/5 water/oil ratio and 1/5 polymer/crosslinker ratio was selected in the present study. Nanogels showed no cell toxicity at various concentrations as characterized by an MTS assay, which is in accordance with Live/Dead assay (Figures S6 and S7, Supporting Information).

It is noteworthy that these nanogels showed high drug-loading efficiency irrespective of formulation due to the drug conjugation to dextran through a pH sensitive bond (Figure S3, Supporting Information). Composite hydrogels were fabricated by mixing the DSNGs in the oxidized dextran solution prior to gel formation, following the addition of dendrimer solution. Fluorescence imaging of the composite hydrogels (with distinct fluorophores to label the hydrogel using FITC and the nanogels using AF 647), revealed that DSNGs were evenly fused into the skeleton of the Dex:Den hydrogels (Figure S8, Supporting Information). Indeed, the presence of sulfur in the composite hydrogels with DSNGs was confirmed by Energy Dispersive X-ray assisted Scanning Electron Microscopy (EDX-SEM) (Figure S9 and Table S2, Supporting Information).

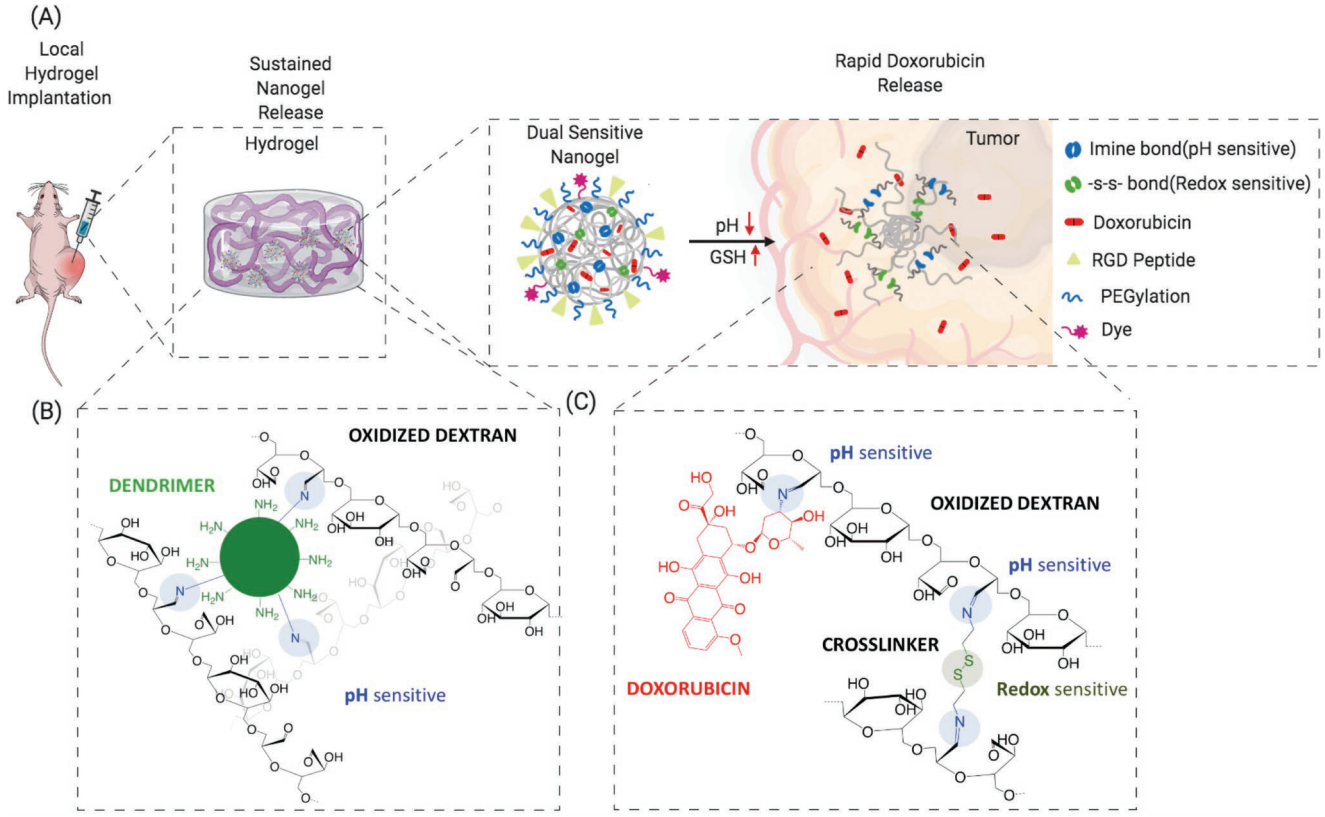

Figure 1. Dual-Sensitive doxorubicin-conjugated nanogels embedded in a hydrogel patch. A) Illustration of the local, hydrogel-assisted sustained delivery of dual-sensitive, doxorubicin-conjugated, nanogels. Nanogels are released over time as the hydrogel degrades. Upon their uptake into cancer cells, doxorubicin is rapidly released due to their dual- stimuli responsive disassembly. B) Chemical structure of the pH sensitive hydrogel patch, composed of oxidized dextran crosslinked with 25% G5-PAMAM dendrimer. C) Chemical structure of the pH- and redox- sensitive nanogels. Cystamine dihydrochloride is used to crosslink the oxidized dextran to form the dual-sensitive nanogels (DSNGs) and hexamethylenediamine is used as a crosslinker to form the nonredox sensitive nanogels (NSNGs).

In vitro release of the nanogels from the hydrogel and then that of the drug from the dual sensitive nanogels (following their uptake in cancer cells) were studied in vitro under different conditions to corroborate the dual triggered release in cancer cells. We quantified drug release mimicking the cancer-cell conditions in the endosome (low pH) and the cytoplasm (GSH), by comparing the release profile under different pH levels (5, 6.5, and 7.4), and with or without a reductive environment (the latter formed by adding GSH, 10×10^{-3} M).[32] We found that the hydrogel provided sustained release of the Dox-containing nanogels, DSNGs, for 20 days (**Figure 2**A). We then studied the release kinetics of the Dox from the DSNGs at different pH levels and with or without GSH, to better understand the release once they will be internalized into cancer cells and exposed to lower pH (Figure 2B) and to GSH (Figure 2C). As imine bond hydrolysis is enhanced under acidic conditions, doxorubicin (Dox)-conjugated dextran nanogels exhibited accelerated release under both pH 6.5 and 5. As shown in Figure 2C, the presence of GSH (10×10^{-3} M) notably accelerated Dox release from the DSNGs, confirming the redox sensitivity of DSNGs. Furthermore, DSNGs were placed in 10×10^{-3} M GSH media with low pH. We hypothesized that the exposure of the Dox-conjugated NGs to the combination of low pH and GSH inside cancer cells would afford rapid release of Dox to initiate cancer-cell killing. Indeed, the release of Dox from the dual-sensitive nanogels (Figure 2D, pH 5 and 10×10^{-3} M GSH) was rapid, with more than 90% released within the first 24 h, compared to 5 days in pH 7.4 without GSH. In summary, in vitro drug release studies provided solid evidence that Dex:Den hydrogels are able to offer sustained release of nanogels (Figure 2A; Figure S4, Supporting Information), while the DSNGs will undergo quick drug dislodge while inside the cancer cells under acidic and redox conditions, providing rapid anticancer therapy.

In order to confirm that the rapid drug release results from the dual triggers—lower endosomal pH and then the cytoplasmic GSH reductive environment—we followed the nanogels- and drug- trafficking within the cell over time. We confirmed that the nanogels were taken up by endocytosis as evident by the colocalization of the nanogels (purple; AlexaFluor 647) with the endosome (green, Lysotracker) (Figure S5, Supporting Information). Then, we studied the uptake of the two types of nanogels (purple; AlexaFluor 647) into cancer cells and the release of doxorubicin (red; autofluorescence at 590 nm) from the nanogels over time (3–12 h) using confocal microscopy (**Figure 3**). Since we expect the DSNGs to degrade and then release doxorubicin faster than the NSNGs, we studied the colocalization of the NGs with the doxorubicin, and

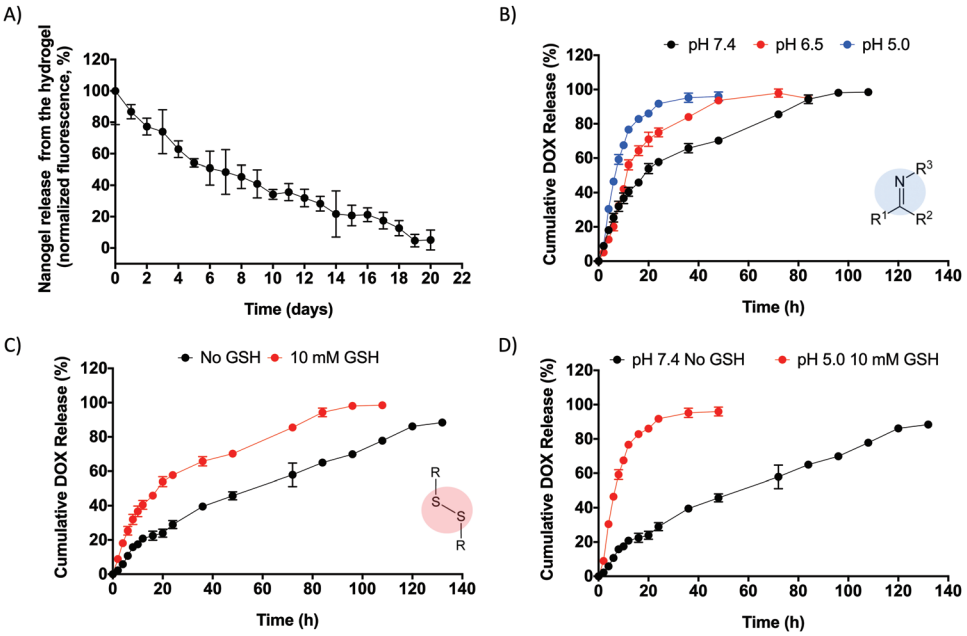

Figure 2. In vitro drug release studies. A) Release of the dual-sensitive nanogels from the composite hydrogels quantified by tracking the fluorescence signal of the labeled nanogels (AF647 dye) over time. B) Release of doxorubicin (DOX) from the nanogels under different pH levels in the presence of 10×10^{-3} M GSH, and C) with or without 10×10^{-3} M GSH at pH 7.4. D) Cumulative release of Dox from the dual-sensitive nanogels under acidic pH and GSH.

then we quantified colocalization of the released doxorubicin with the cell nucleus (blue, DAPI), as is shown in Table S1 in the Supporting Information. At 3 and 6 h, notable amount of doxorubicin was still conjugated to the nanogels (95% and 65%, respectively), while the rest of the drug was found in the nucleus. In contrast, 87% of free doxorubicin was colocalized with the nucleus already after 3 h. However, at 12 h, there was considerably higher release of doxorubicin from the DSNGs compared to the NSNGs, (85% compared to 25% of the doxorubicin was colocalized with the nucleus, respectively). As in early time points both particles are exposed to lower endosomal pH, and are both sensitive to pH degradation, we expect similar amount of drugs to be released. However, once the particles escape the endosome, the high levels of GHS in the cancer cell cytoplasm enhances the release kinetics of doxorubicin from the dual-sensitive nanoparticles, resulting in faster trafficking to the cell nucleus and hence effective cancer-cell death.

To better predict the therapeutic efficacy of the DSNGs in vitro, the uptake of the nanogels—NSNGs or DSNGs—into cancer cells and into control 3T3 cells was evaluated using FACS, and cell viability (IC_{50}) was studied following the delivery of free Dox, and Dox conjugated to either NSNGs or DSNGs. The uptake into both cancer cells and 3T3 cells of either NSNGs or DSNGs alone was comparable (**Figure 4**A). Cell viability of nonloaded DSNGs and NSNGs showed no toxicity in both cell lines (Figures S6 and S7, Supporting Information). However, the IC_{50} was notably different for the two types of Dox-conjugated nanogels when comparing their effect on cancer cells (Figure 4B) and on 3T3 cells (Figure 4C), with significantly higher cancer-cell killing. In particular, at a Dox dose of 100×10^{-9} M, the DSNGs facilitated efficient cancer-cell killing ($IC_{50} = 114 \times 10^{-9}$ M) compared to the NSNGs ($IC_{50} = 296 \times 10^{-9}$ M), while normal 3T3 cells remained intact ($IC_{50} = 2338 \times 10^{-9}$ M for DSNGs and 2354×10^{-9} M for NSNGs). These results suggest that when nanogels are taken up by cancer cells, presenting with high levels of GSH, doxorubicin release is faster and more effective. In contrast, doxorubicin release mechanism in healthy cells, expressing low GSH levels, occur only due to their pH sensitivity. To further corroborate the enhanced effect of DSNGs compared to NSNGs on the efficacy of cancer-cell killing, we blocked the GSH in the cancer cells by treating them with DL-buthionine-sulfoximine (BSO), before determining the IC_{50}. Indeed, blocking GSH resulted in similar IC_{50} for the DSNGs and the NSNGs in cancer cells ($IC_{50} = 318 \times 10^{-9}$ M for DSNGs and 312×10^{-9} M for NSNGs) (Figure 4D).

To ensure proper in vivo delivery of the nanogels either locally in the hydrogel or systemically, we further modified the nanogels with the cell-targeting peptide—RGD[33]- and with PEG chains[34] conjugated to the surface of DSNGs and NSNGs. While PEGylation decreases the uptake into cancer cells, as evident in the higher cell viability in vitro (values 66.7% ± 9.2%), the addition of RGD enabled similar viability to that of unmodified DSNGs (values 37.5% ± 4.3%) (**Figure 5**A), as confirmed by flow cytometry (Figure 5B). Confocal images (Figure 5C) corroborated the uptake of the DSNGs (red, tagged with Alexa Fluor-647) into the cancer cells (blue, DAPI; green, Actin). A strong signal from the nanogels was evident in the cytoplasm and in the perinuclear regions of the cells, which indicates cellular uptake rather than surface anchoring.

We then proceeded to test the efficacy of the biosensitive hydrogel depot in vivo. An orthotopic triple-negative breast cancer was developed in female immunodeficient SCID hairless outbred (SHO, Crl:SHO-Prkdc^{scid}Hr^{hr}, 6 weeks, Charles

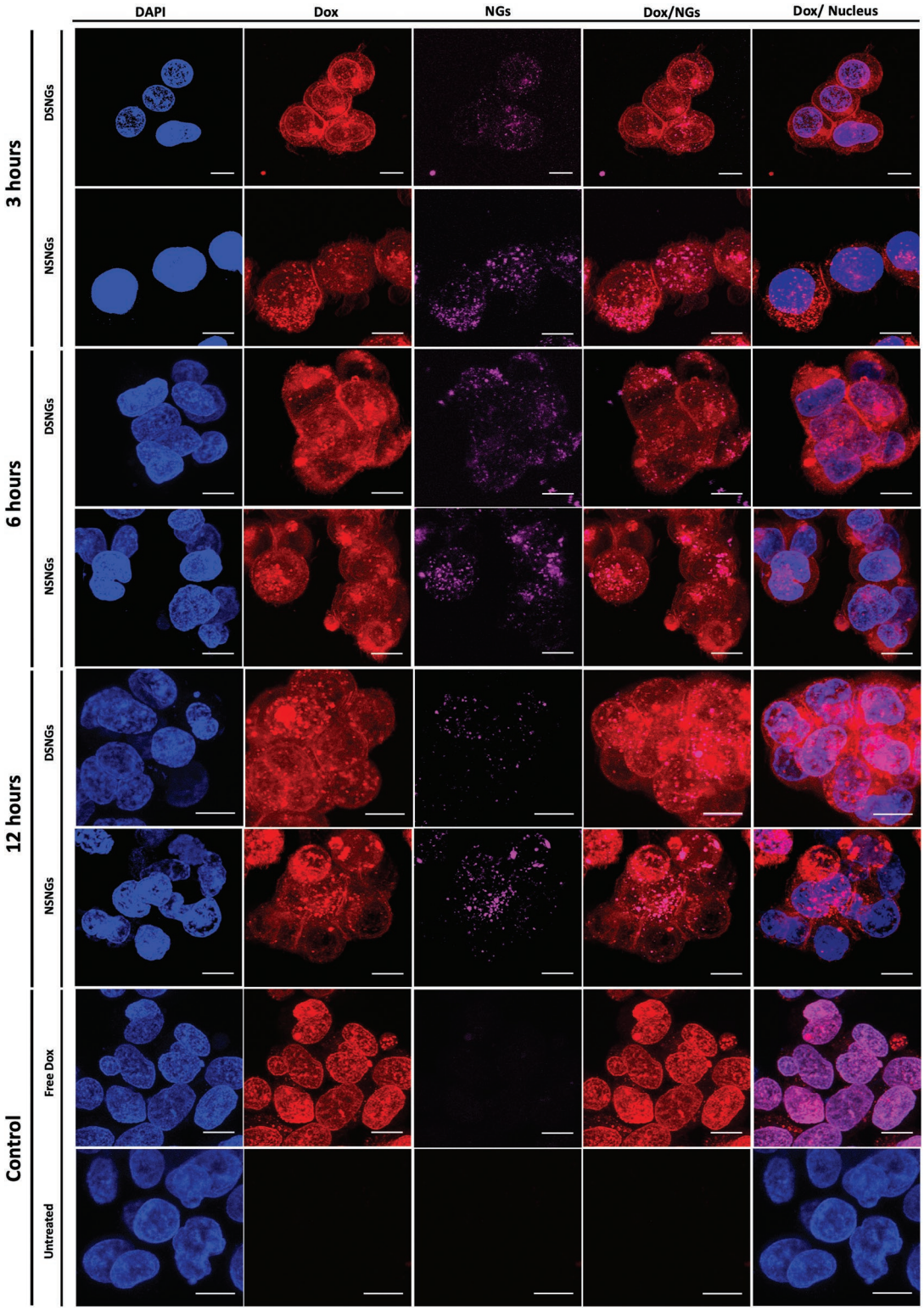

Figure 3. Release kinetics of DOX from DSNGs and NSNGs. Confocal microscopy was used to follow the uptake of the nanogels in MDA-MB-231 cancer cells at different time points, and to follow the release kinetics of DOX from the nanogels. MDA-MB-231 cells were incubated with 5×10^{-6} M DOX-conjugated and AF647-labelled DSNGs or NSNGs. DOX release from the nanogels to the cytoplasm and then migration to the nucleous was analyzed by colocalization studies enabled by the intrinsic DOX fluorescence (red), nanogel labeling (purple) and DAPI staining (blue). Free doxorubicin was used as a positive control and nontreated cells were used as a negative control. Doxorubicin/nucleus colocalization was quantified on maximum intensity projection using ImageJ.

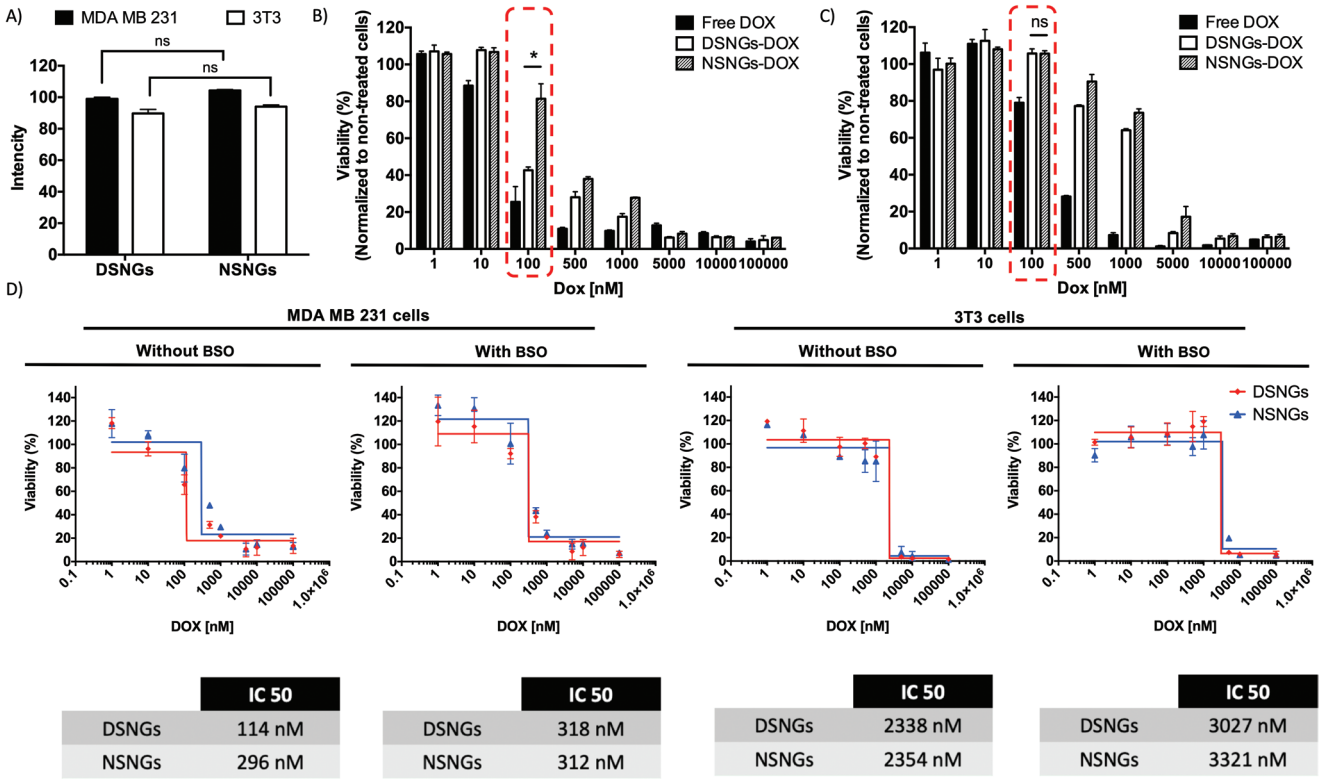

	IC 50
DSNGs	114 nM
NSNGs	296 nM

	IC 50
DSNGs	318 nM
NSNGs	312 nM

	IC 50
DSNGs	2338 nM
NSNGs	2354 nM

	IC 50
DSNGs	3027 nM
NSNGs	3321 nM

Figure 4. In vitro drug dislodge from DSNGs inside cancer cells. Nanogels uptake using labeled DSNGs and NSNGs was carried out in MBA-MD-231 and in normal 3T3 cells and analyzed by flow cytometry A). Nanogels cell-killing effect was studied in vitro using MBA-MD-231 cancer cells and normal 3T3 cells. Cell viability was assessed comparing free doxorubicin, to doxorubicin conjugated to DSNGs and to NSNGs, after 48 h of incubation. B,C) Results were normalized to nontreated cells. D) To corroborate the effect of the dual-sensitivity on cell viability, the effect of DOX release from DSNGs was tested also following glutathione inhibition by exposing MBA-MD-231 cells to DL-buthionine-sulfoximine (BSO, to reduce the glutathione levels), and the IC50 was determined and compared to that of NSNGs. Statistical significance was determined by comparing DSNGs with NSNGs ($*p < 0.05$).

River) mice. MDA-MB-231 cells stably expressing firefly luciferase were used to enable noninvasive and real-time monitoring of the tumor. Mice were injected with luciferin before imaging to assess tumor burden, and all nanogels were labeled with Alexa-fluor 647 prior to administration (**Figure 6**A,B). Both intravenous administration (systemic) of nanogels and on-site (orthotopic tumor) implantation of composite hydrogels (local) have been conducted. For systemic administration, Dox-loaded DSNGs (DSNGs Dox) and Dox-loaded NSNGs (NSNGs Dox) were compared to drug free DSNGs (DSNGs), and saline condition that was used as untreated control. For local administration, biosensitive composite hydrogels with Dox (Hydrogel with DSNGs Dox) were compared to free drug doped DSNGs in the hydrogel (Hydrogel with DSNGs), composite hydrogels with NSNGs containing Dox (Hydrogel with NSNGs Dox), and hydrogels with Dex-conjugated Dox (Hydrogel with Dox). In all the conditions, RGD targeted and PEGylated DSNGs or NSNGs were used for the in vivo study. Biodistribution studies (Figure 6C; Figure S11, Supporting Information) showed that following systemic administration, the nanogels accumulated in the liver and spleen in addition to the tumor site. The enlarged spleen (i.e., splenomegaly) following systemic administration, pointing at drug toxicity, is eliminated when delivered locally. Figure 6D–G showed that groups with drug-free devices (both nanogels and composite hydrogels) had the same tumor size as the negative control at all-time points. This indicated that Dox was solely responsible for the anticancer therapeutic efficacy. Nanogels accumulation at the tumor site peaked at 48 h following systemic delivery and then plummeted rapidly, in all groups, which halted tumor growth in the first 3 days postinjection of NSNGs Dox, however, tumor growth was reinstated rapidly thereafter. A significant reduction of tumor size after 24 h and slow tumor growth up to 72 h were observed in the DSNGs Dox group. The DSNGs conferred more rapid and efficient tumor abrogation than NSNGs due to the fast drug release from the DSNGs within cancer cells, which complies with the results of the in vitro drug release studies (Figure 6F). Despite the initial tumor shrinkage following the systemic administration of the DSNGs, tumor growth accelerated 72 h postinjection. Consecutive administration could be used to further increase their clinical efficiency, however nanogel accumulation in the liver and spleen cannot be avoided, which ultimately will limit their clinical applicability (Figure 6).

The local administration of nanogels (Figure 6E,G) resulted in their persistence in the tumor microenvironment for about 10 days, which was similar to the result observed for the in vitro release of dual-sensitive nanogels from composite hydrogels (Figure 2A). Tumor shrinkage was observed up to 5 days for hydrogel embedded with DSNGs Dox or with NSNGs Dox

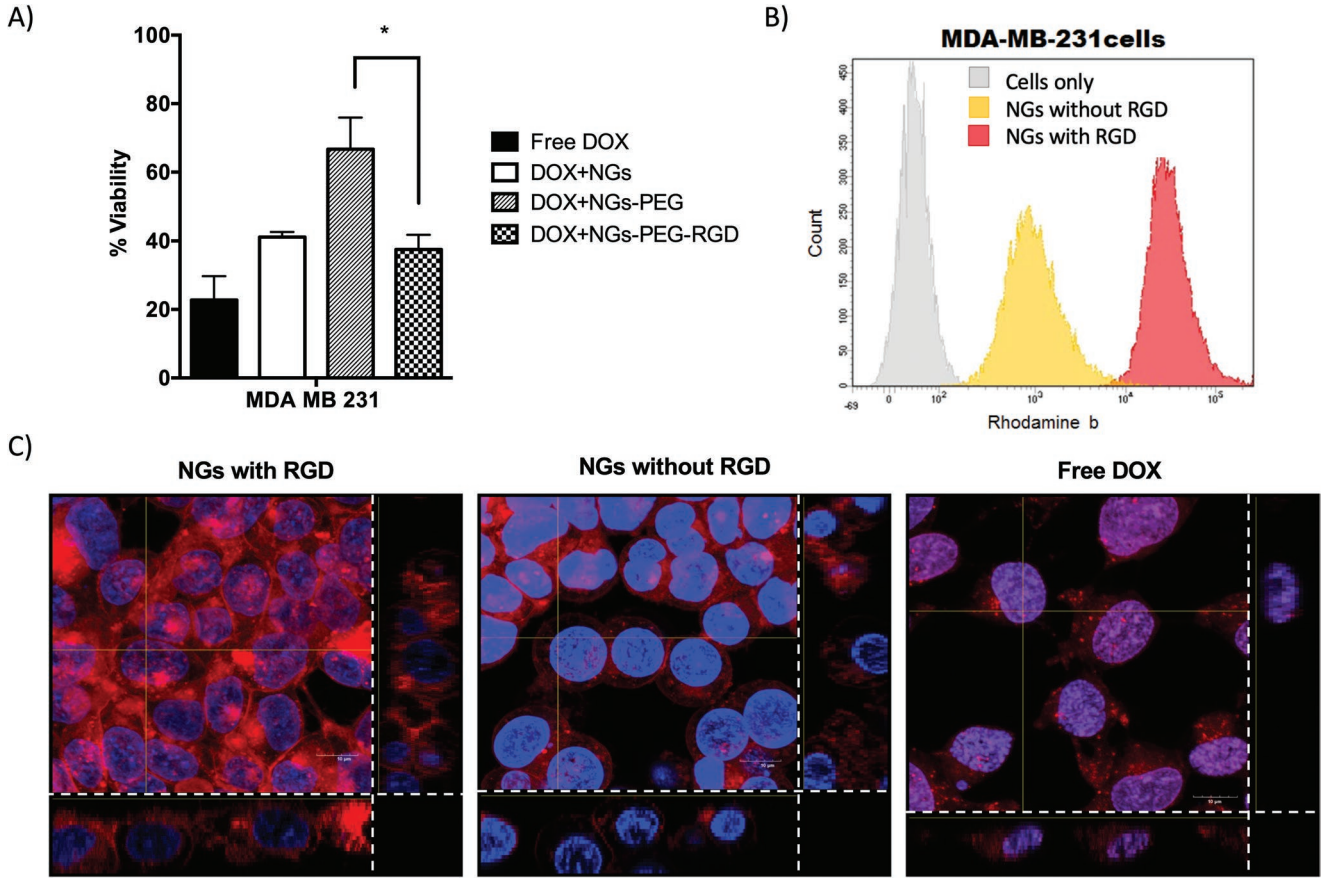

Figure 5. A) Selective uptake of the dual-sensitive nanogels by cancer cells. DSNGs were conjugated with RGD to improve their specificity to cancer cells and the therapeutic efficacy of RGD targeted DSNGs was tested by MTS assay using MDA-MB-231 breast cancer cells. Statistical significance was determined by comparing RGD targeted NGs with nontargeted NGs (*$p < 0.05$). B) Flow cytometry of RGD targeted DSNGs using MDA-MB-231 breast cancer cells. Confocal microscopy images of cellular uptake of nanogels with and without RGD peptide into MDA-MB-231 breast cancer cells after 3 h. Free Doxorubicin was used as a control. C) Nanogels uptake was analyzed by colocalization studies of intrinsic DOX fluorescence (red) and DAPI staining (blue), and orthogonal projection (*z* plane) was performed for all the conditions (the areas outside the white dashed line represent the *z*-stack of the selected cells represented by the intersecting lines).

(Figure 6D), with the exception of hydrogel-conjugated Dox, which results in tumor reduction only in the first two days. Accelerated tumor growth was seen in the Hyd group containing NSNGs Dox after 5 days, while the tumor kept shrinking up to 11 days in the group treated with Hyd containing DSNGs Dox. These results indicate that sustained release combined with rapid drug dislodge inside cancer cells provide with an efficient tumor elimination as seen for the hydrogel group containing DS NGs Dox. In addition, H&E results corroborate that systemic delivery of nanogels do not achieve efficient antitumor efficiency after 11 days of treatment. However, when the nanogels were released in a sustained manner using a locally implanted hydrogel, the nanogels are able to efficiently release the therapeutic drug achieving tumor reduction, which is highly associated with lower tumor vascularization. Therefore, we developed a new delivery platform in which local delivery of doxorubicin can be used as a neoadjuvant chemotherapy for TNBC patients, allowing a fast and near-complete shrinkage of triple negative breast tumors. In addition, systemic delivery of nanogels can be used for advanced stage patients with metastatic disease.

3. Conclusion

The dual-sensitive composite hydrogel—composed of pH- and redox-sensitive dextran-based nanogels embedded within dextran:dendrimer hydrogels—provide sustained release of nanogels from the hydrogel, enhanced nanogel uptake by cancer cells, and rapid release of the chemotherapeutic drug from the nanogels following their uptake into cancer cells. This biosensitive hydrogel depot can be exploited to deliver combination anticancer therapeutics and to treat a range of solid tumors.

4. Experimental Section

Materials: Reagents and solvents were obtained from Sigma–Aldrich. Doxorubicin was purchased from Cayman Chemicals. RGD peptide was synthesized in Biopolymers and Proteomics Core Facility from MIT. MDA MB 231 and 3T3 cell lines were obtained from ATCC (Manassas, VA) and maintained at 37 °C in 5% CO_2 atmosphere in complete DMEM, containing 10% fetal bovine serum, 100 units mL^{-1} penicillin, 100 µg mL^{-1} streptomycin, 0.1×10^{-3} M MEM nonessential amino acids (NEAA), 2×10^{-3} M L-glutamine obtained from Gibco.

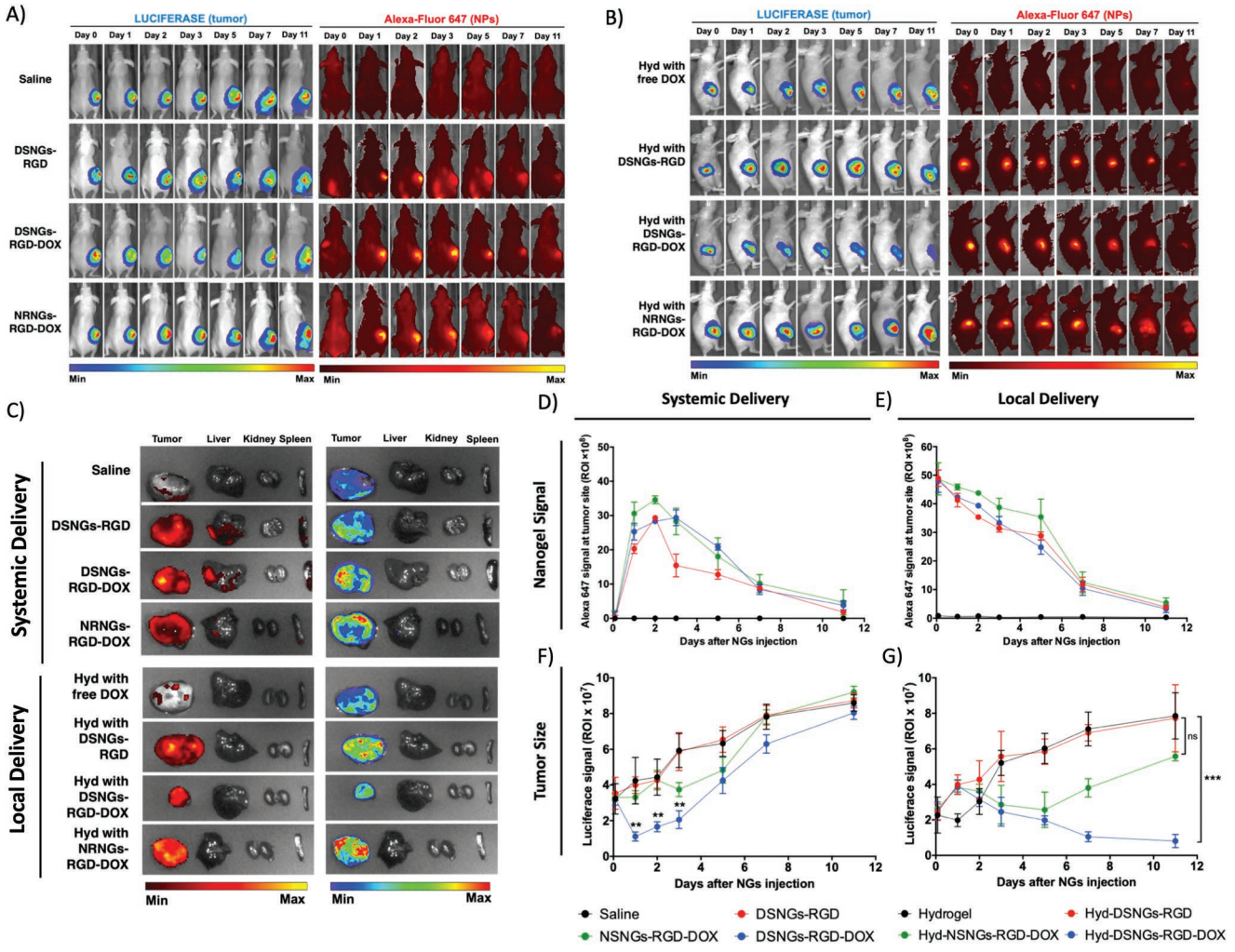

Figure 6. DSNGs enhance tumor shrinkage in vivo. In vivo evaluation of cancer-treatment efficacy following the systemic administration of nanogels and the local administration of composite hydrogel, embedded with nanogels. Tumors were injected with luciferin before imaging, and all nanogels were labeled with AF647 prior to their administration. Tumor progression was studied using in vivo imaging system (IVIS). A) Nanogels accumulation in the tumor and tumor size following systemic administration and B) local administration. C) Epi-fluorescence images of tumor tissue and selected organs after 11 days (blue represent the luciferase signal from the tumor, and red the labeled nanogels). D) Quantitative evaluation of nanogels accumulation in the tumor following systemic administration and E) their retention following local administration. Quantitative evaluation of tumor size at different time points F) following the systemic or G) local administration of the hydrogel formulation. Posthoc test using one-way ANOVA was used to compare DSNGs-RGD-DOX to nontreated mice at 1, 2, and 3 days following systemic delivery and at 11 days after local delivery (*$p < 0.05$; **$p < 0.01$; ***$p < 0.001$).

Dextran Aldehyde Synthesis: Linear dextran (18.9 g, 10 kDa) was dissolved in water with sodium periodate (17.6 g) for 5 h to create dextran aldehyde (50% oxidation of glucose rings, 2 aldehyde groups per oxidized glucose ring). The reaction mixture was dialyzed (MEMBRA-CEL Dialysis Tubing, molecular weight cutoff of 3500 Da, Viskase Companies, Inc.). Dry powder of oxidized dextran was obtained with lyophilization. Chemical structure of oxidize dextran was confirm by ^{1}H-NMR and oxidation degree was determined by hydroxylamine titration assay.

Dextran Aldehyde Labeling: Dextran aldehyde was fluorescently labeled with AlexaFluor 647 Cadaverine (Thermo Fisher). Amine-reactive group in the fluorophore react with aldehyde groups in oxidized dextran to form a reversible imine bond. Then, the imine bond was reduced with sodium cyanoborohydride to produce a stable secondary amine bond between the fluorophore and the dextran aldehyde. Briefly, 10 mg of dextran aldehyde were dissolved in 900 µL of 50×10^{-3} M carbonate buffer (pH 8.5) and 0.3 mg of AF647 dissolved in 100 µL of carbonate buffer were added drop wise and allowed to react for 1 h. Then the reaction mix was cooled down in an ice-water bath and 1.5 mL of 30×10^{-3} M sodium cyanoborohydride solution was added and allowed to react for 3 h. Then, the reaction was dialyzed through a 3000 Da MWCO centrifugal filter (Amicon Ultra-15, EMD Millipore).

Nanogels Synthesis: Doxorubicin loaded nanogels were fabricated by single emulsion technique (**Scheme 1**). Oxidized dextran (10 mg) and doxorubicin (2.9 mg) was dissolved in polyvinyl alcohol (PVA) (5% w/v)

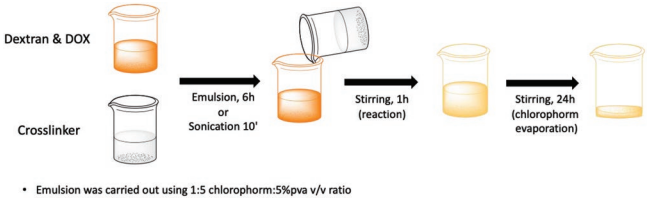

Scheme 1. Fabrication of doxorubicin loaded nanogels via a single emulsion technique.

aqueous solution, and triethylamine (7 µL) was added to form prodrug. Cystamine dihydrochloride (1.126 mg) was used to prepare the DSNGs and was dissolved in PVA solution (0.5 mL, 5% w/v) with 14 µL triethylamine. Both solutions were mixed vigorously with chloroform (volume ratio 1:5) separately, and stirred for 6 h to create emulsion. Two emulsions were mixed and stirred for 1 h for crosslinking. Chloroform was evaporated overnight and the final nanogel was collected. Cystamine dihydrochloride was replaced by hexamethylenediamine to prepare non-redox-sensitive nanogels (NSNGs). Drug free nanogels were fabricated in the same manner without doxorubicin.

Doxorubicin Loading Efficiency Quantification: Nanogels were prepared as previously have been described and nonloaded doxorubicin was dialyzed through a 10 kDa MWCO centrifugal filter (Amicon Ultra-15, EMD Millipore). Nanogels were washed three times with Milli-Q water. Drug loading efficiency was determined by the intrinsic fluorescence of the nonreacted doxorubicin.

Dextran-Dendrimer Hydrogel Formation: Dextran-dendrimer hydrogel formation were prepared as previously have been described.[28] Generation five polyamidoamine (PAMAM) dendrimer with 25% amine surface groups (Dendritech Inc.) was dissolved in water to obtain a 12.5% (w/v) aqueous solution. Dextran aldehyde was also prepared as an aqueous solution (10%, w/v). The two homogeneous polymer solutions were mixed in equal volumes by pipetting and network formation occurred within seconds by Schiff-base reaction between the constituent reactive groups (aldehydes and amines).

Biophysical Characterization: Samples were diluted in PBS 1X and the particle size distribution were determined by laser dynamic light scattering method (DLS) using Nanosizer ZS instrument (Malvern Instruments, UK). Nanogels morphology was observed by Transmission Electron Microscopy (FEI, Tecnai, Multipurpose TEM).

In Vitro Drug Release: In vitro nanogels release behavior from the composite hydrogel and drug release from DS NGs was studied. To assess the release of nanogels from composite hydrogels, DS NGs were conjugated with Alexa Fluor 647 prior to composite hydrogel fabrication, as previously have been described. Composite hydrogels were placed in 48-wells plates, and immersed with releasing media (0.5 mL). Releasing media was replaced at predetermined time point, and fluorescence of the composite hydrogel was measured by Microplate Reader. Nanogel release was assessed checking the fluorescence at 650–665 nm and doxorubicin from the nanogel loaded in the hydrogel was determined by measuring UV absorbance at 480 nm. All release media were PBS based. To assess the release of doxorubicin from DS NGs, 1 mL nanogels were placed in a Dialysis Membranes with 500–1000 molecular weight cut off (Spectrum Laboratories), then immersed into selected releasing media (100 mL). Concentration of Dox in releasing media was determined by measuring UV absorbance at 480 nm by Microplate Reader (Varioskan Flash Multimode Reader, Thermo Scientific). Release studies were carried out at different pH (7.4, 6.5, and 5.0) and/or at different GHS concentrations (0 and 10×10^{-3} M), mimicking the pH-sensitive and redox-sensitive environments.

Cellular Uptake of Fluorescently Labeled Nanogels in MDA-MB-231 and in 3T3 Cells: Cells were seeded in 12-well plates at 100 000 cells per well and incubated overnight to roughly 80% confluence prior to performing the transfection experiments. Nanogels were prepared as described previously and added to the cells at a final concentration of 10×10^{-6} M of Doxorubicin. After 3 h, the remaining nanogels were removed and cells were trypsinized and fixed with paraformaldehyde (PFA) at 1% for flow cytometry analysis. Data was acquired and analyzed by FACS LSR Fortessa HTS-1 (BD Biosciences) flow cytometer.

Viability Assay of DSNGs, NSNGs, and Free Doxorubicin in MDA MB 231 and 3T3 Cell Lines: Cell viability assays of treated cells were performed using the MTS assay (CellTiter 96 AQueous One Solution Cell Proliferation Assay, Promega Corporation, USA) at 48 h post-treatment, as instructed by the manufacturer. Briefly, cells were seeded in 96-well plates at 10 000 cells per well and incubated overnight to roughly 80% confluence prior to performing the transfection experiments. Doxorubicin-loaded nanogels, empty nanogels, and free doxorubicin were added to the cells at different concentration, ranging from 100 000 to 1×10^{-3} M. At 48 h post-treatment, the medium was removed, cells were washed with PBS, and complete medium supplemented with 20% MTS reagent (v/v) was added. Cells were incubated at 37 °C, and absorbance was measured at 490 nm using a microplate reader.

IC_{50} Study of DS NGs and NSNGs in Presence of BSO: MDA MB 231 and 3T3 cells were seeded in 96-well plates at 10 000 cells per well and incubated overnight to roughly 80% confluence prior to performing the transfection experiments. Cells were treated with or without BSO at 1×10^{-3} M for 1 h before the DSNGs and NSNGs treatment. At 48 h after the treatment, cell viability assay was performed using the MTS assay, as previously have been described. IC_{50} of each condition was determined using GraphPad Software.

Nanogel Internalization Studied by Confocal Microscopy: MDA-MB-231 cells were seeded 35 mm dish (P35GCOL-1.5-10-C; from MatTek Corporation) at 150 000 cells per plate and incubated overnight to roughly 50% confluence. Cells were treated using AF647 labeled nanogels loaded with DOX at 5×10^{-6} M for 3 h at 37 °C and 5% CO_2 atmosphere. Subsequently, cells were washed three times with PBS and stained with Lysotracker Green DND-26 and DAPI following the manufacturer protocol. Each fluorescent dye was analyzed with the corresponding filter: DAPI (315–400 nm) in blue; DOX (510–560 nm) in red; Lysotracker (504–511 nm) in green, and AF647 (594–633 nm) in purple.

Nanogel Release Kinetics Mechanism Studied by Confocal Microscopy: In order to study the doxorubicin release mechanism from the newly developed nanogels, MDA-MB-231 cells were treated using AF647 labeled nanogels loaded with DOX. Intrisic DOX fluorescence (red), nanogel fluorescence (purpple) and DAPI staining (blue) were analyzed at 3, 6, and 12 h. Briefly, MDA-MB-231 cells were seeded 35 mm dish (P35GCOL-1.5-10-C; from MatTek Corporation) at 150 000 cells per plate and incubated overnight to roughly 50% confluence. Cells were incubated for 3, 6, or 12 h at 37 °C in a 5% CO_2 atmosphere with nanogels at 5×10^{-6} M. Subsequently, cells were washed three times with PBS and stained with DAPI following the manufacture protocol. Each fluorescent stain was analyzed with the corresponding filter: DAPI (315–400 nm) for blue fluorescence; DOX (510–560 nm) for red fluorescence; and AF647 (594–633 nm) for purple fluorescence. Images of cells were taken with Olympus FV1200 Laser Scanning Confocal Microscope. Doxorubicin/nucleus colocalization was quantified on maximum intensity projection using ImageJ software. Total doxorubicin intensity (mean) was multiplied by total doxorubicin area (% area). Then, the cytoplasm doxorubicin intensity was multiplied by the cytoplasm area (% area) and the nucleus doxorubicin intensity was multiplied by the nucleus area (% area). Then, the percentage of doxorubicin was compared between the nucleus and the cytoplasm.

Cell-Targeting Peptide—RGD and PEG Chain Nanogels Conjugation: Bare nanogels were synthetized as previously have been described. Nanogels surface were further modified with cell-targeting peptide or amine-PEG moieties though Schiff-base reaction between nanogel surface aldehydes with terminal primary amines from RGD peptide or amine-PEG polymer. Nanogels were incubated at 10 mg mL^{-1} in PBS with 35 µg mL^{-1} (1/100 RGD/dextran molar ratio) of RGD peptide and 100 µg mL^{-1} (5/100 amine-PEG/dextran molar ratio) of amine-PEG during 2 h at room temperature. Nonreacted peptide and PEG polymer were dialyzed through a 10 kDa MWCO centrifugal filter (Amicon Ultra-15, EMD Millipore).

RGD Targeted Nanogel In Vitro Assays: For therapeutic efficacy study, MDA MB 231 cells were incubated with Dox-loaded dual sensitive nanogels with or without PEG, and with or without RGD peptide at 100×10^{-9} M. Cell viability was evaluated after 48 h of incubation by MTS assay, as previously have been described. RGD targeting was further analyzed by confocal microscopy and flow cytometry. For confocal microscopy, cells were treated with RGD targeted DS NGs and with nontargeted DS NGs. After 3 h, NGs were removed and cells were fixed with paraformaldehyde (4%) in PBS for 15 min at 37 °C and mounted in ProLong Gold Antifade Reagent with DAPI (Invitrogen) to allow for nuclear staining. Images of cells were taken with a Nikon A1R Ultra-Fast Spectral Scanning Confocal Microscope. For flow cytometry, cells were

treated with RGD targeted DS NGs and with nontargeted DS NGs. After 3 h, the remaining nanogels were removed and cells were trypsinized and fixed with paraformaldehyde (PFA) at 1% for flow cytometry analysis. Data was acquired and analyzed by FACS LSR Fortessa HTS-1 (BD Biosciences) flow cytometer.

Tumor Induction: Orthotopic triple negative breast cancer mice model was developed for in vivo animal study. Tumors in the mammary fat pad were induced in female immunodeficient SCID hairless outbred (SHO) mice by injection of 5×10^6 MDA-MB-231 cells stably expressing firefly luciferase, suspended in HBBS (50 µL) (Lonza) solution. For determination of tumor growth, individual tumors were measured using caliper and tumor volume was calculated by: Tumor volume (mm^3) = width × (length^2)/2. When tumors reached a volume of 0.1 cm^3, mice were randomly sorted into control and experimental groups.

Therapeutic Effect of DSNGs and NSNGs In Vivo: Mice were randomly sorted into control and experimental groups ($n = 5$ for each group). Nanogels were administered both systemically and locally. For systemic administration mice were injected with DSNGs with DOX at 3 mg mL^{-1}, NSNGs with DOX at 3 mg mL^{-1}, DSNGs without DOX at 3 mg mL^{-1}, and Saline solution via tail-vein and the tumor growth was followed during 11 days. For local administration, pre-cured disks of hydrogel scaffold embedded with nanogels were formed and implanted subcutaneously on top of the fat mammary tumor in SCID mice and the tumor growth was followed during 11 days. Free DOX loaded hydrogel, DSNGs with DOX loaded hydrogel, NSNGs with DOX loaded hydrogel, and DSNGs without DOX loaded hydrogel were used. For local hydrogel implantation, syringes, mixing tips and needles used were autoclaved and for all experimental groups, solutions were sterilized through 0.2 µm filters. For analysis of tumor growth, noninvasive longitudinal monitoring of tumor progression was followed by scanning mice with the IVIS Spectrum-bioluminescent and fluorescent imaging system (Xenogen XPM-2 Corporation) from mice bearing mammary tumors from luciferized MDA-MB-231 cells ($n = 5$ animals per treated group). 15 min before imaging, mice were intraperitoneally injected with D-luciferin (150 µL, 30 mg mL^{-1}, Perkin Elmer) in DPBS (Lonza). Whole-animal imaging was performed during 11 days. At the end of 11 days mice were sacrificed and the organs harvested and imaged. All experimental protocols were approved by the MIT Animal Care and Use Committee and were in compliance with NIH guidelines for animal use.

H&E Staining: Tumors were resected from the SCID SHC mice and kept at –80 °C for a minimum time of 24 h. Then, tumors were embedded with O.C.T and cryosectioned with Leica CM 1850 Cryotome to yield 9 µm tissue slides. Hematoxylin and Eosin Stain was performed following standard protocols. Hematoxylin, Mayer's and Eosin Y solution (Vector Laboratories) were used to stain the nuclei and cytoplasm/erythrocytes respectively. Samples were analyzed by phase contrast microscopy (Nikon Confocal Microscope) and images were processed using ImageJ software.

Statistical Analysis: All values were expressed as mean ± standard deviation. Statistical differences were analyzed with GraphPad Prism 5. The unpaired Student's t-test was used to test statistical difference between two measurements. Posthoc test for one-way ANOVA was used to test statistical difference between sets of measurements (*$p < 0.05$; **$p < 0.01$; ***$p < 0.001$).

Supporting Information

Supporting Information is available from the Wiley Online Library or from the author.

Acknowledgements

Y.Z. and P.D. contributed equally to this work. The authors thank the Swanson Biotechnology Center at the Koch Institute for Integrative Cancer Research at Massachusetts Institute of Technology (MIT) for assistance with animal experiments and facilities, especially the microscopy, flow cytometry, and histology cores. The authors thank D. S. Yun for cryo-TEM assistance at the Peterson Nanotechnology Materials Core Facility. The authors thank the Department of Comparative Medicine at MIT, especially J. Haupt. The authors thank G. Paradis for FACS assistance with Cancer Center Support (FACS core). The authors thank Eliza Vasile for microscopy assistance in the core microscopy core. The authors thank Alexander Bradford Austin for the synthesis of peptides in the core of Biopolymers & Proteomics Core at the Koch Institute for Integrative Cancer Research at Massachusetts Institute of Technology (MIT).

Conflict of Interest

The authors declare no conflict of interest.

Keywords

breast cancer, composite hydrogels, dual sensitive nanogels, pH sensitivity, redox sensitivity

Received: August 13, 2019
Revised: December 9, 2019
Published online:

[1] G. V Echeverria, Z. Ge, S. Seth, X. Zhang, S. Jeter-Jones, X. Zhou, S. Cai, Y. Tu, A. McCoy, M. Peoples, Y. Sun, H. Qiu, Q. Chang, C. Bristow, A. Carugo, J. Shao, X. Ma, A. Harris, P. Mundi, R. Lau, V. Ramamoorthy, Y. Wu, M. J. Alvarez, A. Califano, S. L. Moulder, W. F. Symmans, J. R. Marszalek, T. P. Heffernan, J. T. Chang, H. Piwnica-Worms, *Sci. Transl. Med.* **2019**, *11*, eaav0936.
[2] J. Conde, N. Oliva, N. Artzi, *Proc. Natl. Acad. Sci. USA* **2015**, *112*, E1278.
[3] X. Liang, C. Chen, Y. Zhao, P. C. Wang, in *Circumventing Tumor Resistance to Chemotherapy by Nanotechnology* (Ed: J. Zhou), Humana Press, Totowa, NJ **2010**, pp. 467–488.
[4] A. Z. Wang, R. Langer, O. C. Farokhzad, *Annu. Rev. Med.* **2012**, *63*, 185.
[5] S. M. Janib, A. S. Moses, J. A. MacKay, *Adv. Drug Delivery Rev.* **2010**, *62*, 1052.
[6] H. T. Ta, C. R. Dass, D. E. Dunstan, *J. Controlled Release* **2008**, *126*, 205.
[7] N. A. Peppas, K. M. Wood, J. O. Blanchette, *Expert Opin. Biol. Ther.* **2004**, *4*, 881.
[8] N. S. Satarkar, D. Biswal, J. Z. Hilt, *Soft Matter* **2010**, *6*, 2364.
[9] J. V Jokerst, T. Lobovkina, R. N. Zare, S. S. Gambhir, *Nanomedicine* **2011**, *6*, 715.
[10] X. H. Gao, Y. Y. Cui, R. M. Levenson, L. W. K. Chung, S. M. Nie, *Nat. Biotechnol.* **2004**, *22*, 969.
[11] F. Alexis, E. Pridgen, L. K. Molnar, O. C. Farokhzad, *Mol. Pharmaceutics* **2008**, *5*, 505.
[12] N. Kamaly, Z. Y. Xiao, P. M. Valencia, A. F. Radovic-Moreno, O. C. Farokhzad, *Chem. Soc. Rev.* **2012**, *41*, 2971.
[13] O. P. Varghese, W. L. Sun, J. Hilborn, D. A. Ossipov, *J. Am. Chem. Soc.* **2009**, *131*, 8781.
[14] T. R. Hoare, D. S. Kohane, *Polymer* **2008**, *49*, 1993.
[15] S. A. Meenach, J. Z. Hilt, K. W. Anderson, *Acta Biomater.* **2010**, *6*, 1039.
[16] J. Z. Du, X. J. Du, C. Q. Mao, J. Wang, *J. Am. Chem. Soc.* **2011**, *133*, 17560.

[17] E. S. Lee, K. Na, Y. H. Bae, *J. Controlled Release* **2005**, *103*, 405.
[18] E. S. Lee, Z. G. Gao, Y. H. Bae, *J. Controlled Release* **2008**, *132*, 164.
[19] K. S. V. K. Rao, Q. Zhong, E. R. Bielski, S. R. P. da Rocha, *Mol. Pharmaceutics* **2017**, *14*, 3866.
[20] J.-P. Behr, *Chimia* **1997**, *51*, 34.
[21] A. Russo, W. Degraff, N. Friedman, J. B. Mitchell, *Cancer Res.* **1986**, *46*, 2845.
[22] N. Oliva, M. Carcole, M. Beckerman, S. Seliktar, A. Hayward, J. Stanley, N. M. A. Parry, E. R. Edelman, N. Artzi, *Sci. Transl. Med.* **2015**, *7*, 272ra11.
[23] N. Artzi, T. Shazly, A. B. Baker, A. Bon, E. R. Edelman, *Adv. Mater.* **2009**, *21*, 3399.
[24] Z. Sideratou, D. Tsiourvas, C. M. Paleos, *Langmuir* **2000**, *16*, 1766.
[25] J. Conde, N. Oliva, Y. Zhang, N. Artzi, *Nat. Mater.* **2016**, *15*, 1128.
[26] N. Oliva, J. Conde, K. Wang, N. Artzi, *Acc. Chem. Res.* **2017**, *50*, 669.
[27] A. Gilam, J. Conde, D. Weissglas-Volkov, N. Oliva, E. Friedman, N. Artzi, N. Shomron, *Nat. Commun.* **2016**, *7*, 12868.
[28] N. Oliva, S. Shitreet, E. Abraham, B. Stanley, E. R. Edelman, N. Artzi, *Langmuir* **2012**, *28*, 15402.
[29] N. Artzi, N. Oliva, C. Puron, S. Shitreet, S. Artzi, A. B. Ramos, A. Groothuis, G. Sahagian, E. R. Edelman, *Nat. Mater.* **2011**, *10*, 704.
[30] P. Liu, B. H. Shi, C. X. Yue, G. H. Gao, P. Li, H. Q. Yi, M. X. Li, B. Wang, Y. F. Ma, L. T. Cai, *Polym. Chem.* **2013**, *4*, 5793.
[31] D. Xiao, H. Z. Jia, J. Zhang, C. W. Liu, R. X. Zhuo, X. Z. Zhang, *Small* **2014**, *10*, 591.
[32] Y. J. Pan, Y. Y. Chen, D. R. Wang, C. Wei, J. Guo, D. R. Lu, C. C. Chu, C. C. Wang, *Biomaterials* **2012**, *33*, 6570.
[33] J. Conde, F. R. Tian, Y. Hernandez, C. C. Bao, D. X. Cui, K. P. Janssen, M. R. Ibarra, P. V Baptista, T. Stoeger, J. M. de la Fuente, *Biomaterials* **2013**, *34*, 7744.
[34] M. Ogris, S. Brunner, S. Schuller, R. Kircheis, E. Wagner, *Gene Ther.* **1999**, *6*, 595.

